Paper pa02-076
Submitted to the 28th International Conference on High Energy Physics
ICHEP'96, Warsaw, Poland, July 1996

# Measurement of Charged Particle Transverse Momentum Spectra in Deep Inelastic Scattering

H1 Collaboration

**Abstract**

Transverse momentum spectra of charged particles are measured as a function of the kinematic variables $x_B$ and $Q^2$ using the H1 detector at the $ep$ collider HERA. The data are compared to different parton emission models, which are either ordered or unordered in transverse momentum $k_T$ . The data provide evidence for a relatively large amount of parton radiation between the current and the remnant system.

# 1 Introduction

The electron-proton collider HERA allows the exploration of a new kinematic region in deep inelastic scattering (DIS) down to very small Bjorken-$x$ of $\approx 10^{-5}$, where new dynamic features of QCD may show up. So far the description of the nucleon structure function data by perturbative QCD, cast into the DGLAP (Dokshitzer-Gribov-Lipatov-Altarelli-Parisi) parton evolution equations [1], has been extremely succesful, and constitutes one of the major successes of QCD. At small enough $x$ however, these equations are expected to be invalid. For the small $x$ regime the BFKL (Balitsky-Fadin-Kuraev-Lipatov) equation [2] has been postulated, and it would be very interesting to test QCD in such a new regime. At lowest order the BFKL and DGLAP equations resum the leading logarithmic $(\alpha_s \ \ln 1/x)^n$ or $(\alpha_s \ \ln(Q^2 \ /Q_0^2))^n$ contributions respectively. In these approximations the leading diagrams are of the ladder type (Fig. 1). The leading log DGLAP resummation corresponds to a strong ordering of the transverse momenta $k_T$ (w.r.t. the proton beam) in the parton cascade ($Q_0^2 \ll {k_T}_1^2 \ll ...{k_T}_i^2 \ll ...Q^2$ ), while in the BFKL regime the transverse momenta rather follow a kind of random walk (${k_T}_i^2 \approx {k_T}_{i+1}^2$) [3]. Here $Q_0^2$ is the cut-off for the perturbative evolution.

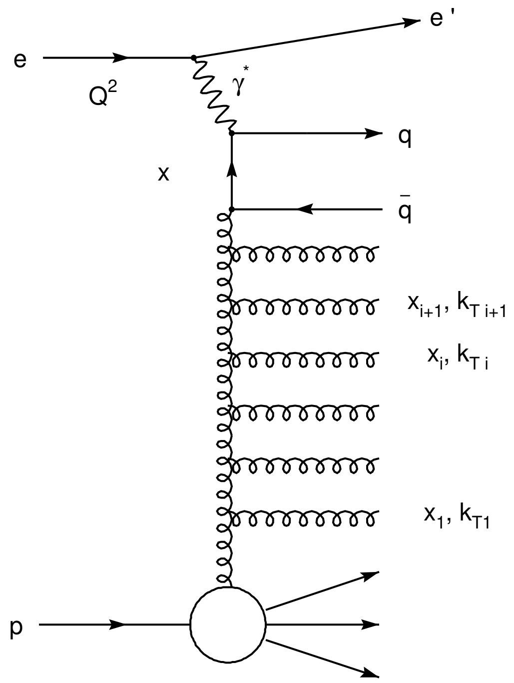


Figure 1: *Generic diagram for parton evolution.*

The strong rise towards small $x$ of the structure function $F_2$ measured at HERA [4, 5] is consistent with the BFKL expectation, but can be described also with conventional DGLAP evolution [6, 7]. Less inclusive measurements, namely of the hadronic final state emerging from the cascade, may offer a better handle to search for BFKL signatures. One example is the production of transverse energy $E_T$ in a region between the current region and the proton remnant [8]. As a consequence of the strong $k_T$ ordering, DGLAP evolution is expected to produce less $E_T$ than the BFKL evolution [9]. The HERA $E_T$ flow data [10] can be interpreted consistently within the BFKL framework, but from those data alone it was not possible to disentangle non-perturbative hadronization effects from perturbative parton radiation, precluding an unambiguous test of the underlying parton dynamics [11, 12]. In fact, the data could also be described with a DGLAP based parton shower model under the assumption of large hadronization effects [12].

In this paper complementary measurements of charged particle transverse momentum ($p_T$) spectra will be presented. Such spectra have been proposed as a more direct probe of the underlying parton dynamics than the $E_T$ flow measurements [13]. For the $k_T$ unordered scenario a harder $p_T$ spectrum is expected than for the $k_T$ ordered evolution, because parton emissions are less restricted in $k_T$ . The unsuppressed gluon radiation should give rise to a hard tail of the $p_T$ distribution for the hadrons emerging from the cascade. The measurements are compared to predictions from Monte Carlo models with different mechanisms for gluon radiation. They incorporate QCD evolution in different approximations and utilize phenomenological models for the non-perturbative hadronization phase.

The MEPS model (Matrix Element plus Parton Shower), an option of the LEPTO generator [14], incorporates the QCD matrix elements up to first order, with additional soft emissions generated by adding leading log DGLAP parton showers. Though this approach is widely used with considerable success, it has to be pointed out that the DGLAP formalism was derived for the totally inclusive structure function evolution, and it can be questioned whether it is fully applicable for exclusive final states [12]. In the colour dipole model (CDM) [15] as implemented in ARIADNE [16], radiation stems from colour dipoles formed by the colour charges. Both programs use the Lund string model [17] for hadronizing the partonic final state. The HERWIG model [18] is also based upon leading log parton showers, with additional matrix element corrections [19]. This model implements an alternative (cluster) fragmentation scheme [20]. The CDM description of gluon emission is similar to that of the BFKL evolution, because the gluons emitted by the dipoles do not obey strong ordering in $k_T$ [21]. In the MEPS and HERWIG models the partons emitted in the cascade are strongly ordered in $k_T$ , because they are based upon leading log DGLAP parton showers. The models are used in their latest versions (LEPTO 6.4 for MEPS, ARIADNE 4.08 for CDM and HERWIG 5.8d), together with the parton density parametrization GRV [7]. They provide a satisfactory overall description of current DIS final state data [22], in particular of the $E_T$ flows [1] For this analysis the use of the alternative parametrization MRS-H [24] would give slightly different, but similar model predictions.

[1] However, in LEPTO the new concept of soft colour interactions [12] had to be introduced to reproduce the level of $E_T$ seen in the data [8, 22, 12]. Intriguingly, this mechanism also produces rapidity gap events [23] at a rate comparable to observation [12], about 10%. Also the cluster fragmentation scheme in HERWIG produces rapidity gap events. In this paper rapidity gap events are excluded.

## 2 Detector Description

A detailed description of the H1 apparatus can be found elsewhere [25]. The following briefly describes the detector components relevant to this analysis.

The hadronic energy flow and the scattered positron are measured with a liquid argon (LAr) calorimeter and a backward electromagnetic lead-scintillator calorimeter (BEMC). The LAr calorimeter [26] extends over the polar angular range $4^\circ < \theta < 153^\circ$ with full azimuthal coverage, where $\theta$ is defined with respect to the proton beam direction ($+z$ axis). It consists of an electromagnetic section with lead absorbers and a hadronic section with steel absorbers. Both sections are highly segmented in the transverse and longitudinal directions with about 44000 cells in total. The total depth of both calorimeters varies between 4.5 and 8 interaction lengths for $\theta < 125^\circ$. Test beam measurements of the LAr calorimeter modules show an energy resolution of $\sigma_E/E \approx 0.50/\sqrt{E\ [\mathrm{GeV}]} \oplus 0.02$ for charged pions [27]. The absolute scale of the hadronic energy measurement is presently known to 5%, as determined from studies of the transverse momentum ($p_T$) balance in DIS events.

The BEMC [28] (depth of 22.5 radiation lengths or 1 interaction length) covers the backward region of the detector, $151^\circ < \theta < 174.5^\circ$. A major task of the BEMC is to trigger and to measure scattered positrons in DIS processes with $Q^2$ values ranging from 5 to 100 GeV$^2$. The BEMC energy scale for electrons is known to an accuracy of 1%. Its resolution is given by $\sigma_E/E = 0.10/\sqrt{E\ [\mathrm{GeV}]} \oplus 0.42/E[\mathrm{GeV}] \oplus 0.03$ [28]. A backward proportional chamber (BPC), in front of the BEMC with an angular acceptance of $155.5^\circ < \theta < 174.5^\circ$ serves to identify electrons and to precisely measure their direction. Using information from the BPC, the BEMC and the reconstructed event vertex the polar angle of the scattered positron is known to a precision of 1 mrad.

The calorimeters are surrounded by a superconducting solenoid which provides a uniform magnetic field of 1.15 T parallel to the beam axis in the tracking region.

The central tracking system is mounted concentrically around the beam line, covering polar angles of $20^\circ < \theta < 160^\circ$. Charge and momenta of charged particles are measured by two coaxial cylindrical drift chambers (central jet chamber, CJC), providing up to 56 space points in the radial plane. Longitudinal coordinates are obtained via charge division from the CJC, and from dedicated drift chambers which are interleaved with the CJC. The achieved resolutions are $\sigma_{p_T}/p_T \approx 0.009 \cdot p_T\ [\mathrm{GeV}] \oplus 0.015$ and $\sigma_\theta = 20$ mrad [25]. The central tracking system is complemented by the forward tracker, which covers polar angles of $7^\circ < \theta < 25^\circ$.

Scintillation counters installed behind the BEMC are used to reject proton induced background. Small angle electron/photon taggers are used for luminosity measurements and the study of photoproduction background.

## 3 Event and Track Selection

The data used in this analysis were collected in 1994, with positrons of energy $E_e$ = 27.5 GeV colliding with protons of energy $E_p$ = 820 GeV, resulting in a total centre of mass energy of $\sqrt{s}$ = 300 GeV . The data correspond to an integrated luminosity of 1.3 $\mathrm{pb}^{-1}$. For this analysis DIS events with $5 < Q^2 < 50$ GeV$^2$ are used, in which the scattered positron is observed in the BEMC. The events are triggered by requiring a cluster of more than 4 GeV in the BEMC. After reconstruction, DIS events are selected in the following way:

- The scattered positron, defined as the most energetic BEMC cluster, must have an energy $E'_e$ larger than 12 GeV and a polar angle $\theta_e$ below 173° in order to ensure high trigger efficiency and a small photoproduction background [4].

- The lateral size of the positron cluster, calculated as the energy weighted radial distance of the cells from the cluster centre, has to be smaller than 4 cm. The cluster must be associated with a reconstructed BPC space point which must lie within 3.5 cm of the cluster centre of gravity. Further reduction of photoproduction background and the removal of events in which an energetic photon is radiated off the incoming positron is achieved by requiring $\sum_j (E_j - p_{z,j}) > 30$ GeV [4], with the sum extending over all particles $j$ (measured calorimetrically) of the event.

- The radial coordinate of the BPC hit must be less than 60 cm, corresponding to an positron angle above 157° with respect to the nominal interaction point, ensuring full containment of the positron shower in the BEMC.

- The $z$ position of the event vertex reconstructed from charged tracks has to be within 30 cm of the average of all collision events.

- The energy in the forward region ($4.4° < \theta < 15°$) has to be larger than 0.5 GeV in order to exclude diffractive-like events with large rapidity gaps in the forward region [23, 8].

- Remaining background is rejected by requiring no veto from the time-of-flight counters.

The kinematic variables are determined using information from the scattered positron: $Q^2 = 4\, E_e\, E'_e \cos^2(\theta_e/2)$ and $y = 1 - (E'_e/E_e) \cdot \sin^2(\theta_e/2)$. The scaling variable $x$ is then derived via $x = Q^2/(ys)$, and the hadronic invariant mass squared is $W^2 = sy - Q^2$.

- As the precision of the $y$ measurement degrades with $1/y$, a cut $y > 0.05$ is imposed. Events suffering from QED radiation or from a badly reconstructed positron are removed by requiring that they also fulfil this cut if $y$ is calculated from the measured hadrons.

For this analysis, only charged particle tracks measured in the CJC are used. They are required to be fit to the primary vertex and their polar angle must lie between 20 and 155 degrees. The upper limit also excludes the scattered positron. A radial track length of at least 10 cm is required to ensure good momentum resolution. By demanding the track to start in the inner jet chamber, tracks are rejected in which the track segments in inner and outer CJC are not linked. After having selected such high quality tracks, the efficiency for finding a genuine primary track is better than 93%.

| Kin.bin | $x$ /$10^{-3}$ | $Q^2$ / GeV$^2$ | $\langle x \rangle$ /$10^{-3}$ | $\langle Q^2 \rangle$/ GeV$^2$ | $< W^2 >$ / GeV$^2$ | #events |
|---|---|---|---|---|---|---|
| 0 | 0.1–10 | 5–50 | 1.14 | 18.3 | 24975 | 59463 |
| 1 | 0.1–0.2 | 5–10 | 0.16 | 7.0 | 45296 | 4853 |
| 2 | 0.2–0.5 | 6–10 | 0.29 | 8.8 | 31686 | 6294 |
| 3 | 0.2–0.5 | 10–20 | 0.37 | 13.1 | 36893 | 9564 |
| 4 | 0.5–0.8 | 10–20 | 0.64 | 14.0 | 22401 | 7129 |
| 5 | 0.8–1.5 | 10–20 | 1.1 | 14.3 | 13498 | 7964 |
| 6 | 1.5–4.0 | 10–20 | 2.1 | 15.3 | 7543 | 4720 |
| 7 | 0.5–1.4 | 20–50 | 0.93 | 28.6 | 32390 | 8349 |
| 8 | 1.4–3.0 | 20–50 | 2.1 | 31.6 | 16025 | 6752 |
| 9 | 3.0–10 | 20–50 | 4.4 | 34.7 | 8225 | 3838 |

Table 1: The kinematic intervals and the average $x$,$Q^2$ and $W^2$ from the raw data. The number of events surviving the selections are given.

# 4 Results

The results are presented for the hadronic centre of mass system (CMS), that is the rest system of the proton and the exchanged boson, where the direction of the exchanged boson defines the positive $z'$ axis. The event sample has been divided into 9 different kinematic bins, resulting in three slices with constant $Q^2$ and varying $x$ (see Table 1). The same binning had been used for the measurement of transverse energy flows [10].

The data are corrected bin-by-bin for detector effects, including photon conversions and secondary interactions, geometrical acceptance and for decay products of particles with a lifetime greater than 8 ns (e.g. $K_s^0 \to \pi^+\pi^-$ and $\Lambda \to p\pi$), as well as for QED radiative effects. The corrections have been determined with Monte Carlo generated events [2] and a full simulation of the H1 detector response. The detector simulation has been checked by comparing in great detail distributions of track quality properties to the data. From an eye scan of tracks in real and in simulated events one can conclude that the tracker efficiency is simulated to an accuracy of better than 2%. No spurious tracks due to noise hits have been found.

Transverse momentum spectra are measured for the pseudorapidity interval $1.5 < \eta < 2.5$, where $\eta = -\ln\tan(\theta/2)$, and $\theta$ is the angle w.r.t. the virtual photon direction. The lower $\eta$ limit is determined by the requirement of good acceptance in all 9 kinematic bins, and the upper limit restricts the measurement to a region away from the current fragmentation region, where significant differences between the different QCD evolution scenarios are expected [13].

The measured spectra, steeply falling with $p_T$ , are shown in Fig. 2 for the nine kine-

[2]The event generator was DJANGO 6.0 [29], based upon HERACLES [30] for the electroweak part and ARIADNE [16] for the QCD part. The simulated/reconstructed events obtained using DJANGO describe the raw data spectra very well. Differences in the correction factors obtained with the alternative model LEPTO, which describes the data less well, are reflected in the systematic errors.

matic bins, and for the combined event sample. The distributions in this paper are always normalized to the number of events $N$ that enter the distribution. The inner error bar represents the statistical error, and the outer error bar the quadratic sum of statistical and systematic errors. We first discuss the systematic errors, and then turn to a discussion of the results.

In most cases, the corrections applied are smaller than 10%, and never exceed 50%. The $p_T$ bins are chosen much larger than the experimental resolution, and bin centre corrections have been applied. Major corrections are due to event migration effects and track selection cuts, contributing mostly at large $p_T$ , and detector acceptance contributing at small $p_T$ . Sources of systematic uncertainties are given in the following:

- Model dependent (ARIADNE vs. LEPTO) acceptance corrections can differ by as much as 20 %, but in general not more than 5 %.
- Track selection cuts have been varied, leading to a 10% uncertainty for particles with $p_T < 0.5$ GeV , and for the kinematic bins at low $W$, where one measures close to the limit of the detector acceptance.
- There may be a contamination of up to 5% from photoproduction for the kinematic bins at large $W$ [31]. In order to estimate the uncertainty due to the contamination, stricter electron quality cuts have been applied at the cost of statistics, and events have been rejected with signals in the electron/photon taggers. Differences in the result obtained w.r.t. the standard selection are reflected in the systematic error.
- The uncertainty of the BEMC energy scale affects the boost to the CMS and event migration effects. However, the effect is negligible for all bins except for the bins at large $x$ and $Q^2$ , where it may give rise to an uncertainty up to 15 %. The boost to the CMS introduces a well understood correction of less than 10 % for the low $Q^2$ sample discussed here.
- The relative calibration between inner and outer drift chamber was checked by comparing the $p_T$ spectra of positively and negatively charged tracks. No significant difference was found.

The $p_T$ spectra are compared to the models ARIADNE, LEPTO and HERWIG, representing the suppressed (LEPTO, HERWIG) and unsuppressed (ARIADNE) gluon radiation scenarios. At "large" $x$ and $Q^2$ (here "large" means $Q^2 \approx 35$ GeV$^2$ and $x \approx 0.004$) all models provide a good description of the data. At smaller $x$ and $Q^2$ , LEPTO and HERWIG fall significantly below the data for $p_T > 1$ GeV . ARIADNE gives a good description of the data over the full kinematic range. Following the arguments in [13], the hardness of the $p_T$ spectra is a measure of parton radiation. The shortfall of the models with suppressed gluon radiation indicates that at small $x$ there is more parton radiation present than is produced by the models based upon leading log DGLAP parton showers. The data are well described by the model ARIADNE in which parton radiation is more abundant.

In order to check the predicted hardening of the $p_T$ spectrum with decreasing $x$ due to increasing gluonic activity [13], the $p_T$ spectra are compared in Fig. 4 a for the highest and lowest $x$ bins (differing by a factor 6 in $x$ ) of the intermediate $Q^2$ ($\approx$ 14 GeV$^2$ ) slice. There is a trend consistent with the prediction, however not very significant. Because $W^2 \approx Q^2/x$, this effect can also be understood as a $W$ dependence.

From a comparison of bins 2 and 7 (Fig. 4 b), where $W^2$ is fixed ($\approx$ 32000 GeV$^2$ ) and $Q^2$ varies by a factor 3 (from 9 to 29 GeV$^2$ ), it can be seen that the $p_T$ spectrum becomes harder with increasing $Q^2$ . When $x$ is fixed ($x = 0.0021$), and $Q^2$ increased by a factor 2, the $p_T$ spectrum becomes also harder, see Fig. 4 c. We have observed previously that in the current fragmentation region the transverse energy $E_T$ increases with $Q^2$ for fixed $W$ [32]. That $Q^2$ dependence diminishes towards the proton remnant. The $E_T$ measured in the interval $1.5 < \eta < 2.5$ still increases slightly with $Q^2$ . In the central interval $-0.5 < \eta < 0.5$ no $Q^2$ dependence of $E_T$ was seen for $Q^2 < 50$ GeV$^2$ . The CJC acceptance does not allow to check the $Q^2$ dependence of the $p_T$ spectra in the same central $\eta$ interval. To summarize, at fixed $Q^2$ there appears to be a hardening of the $p_T$ spectrum with decreasing $x$ and correspondingly increasing $W$ , while at fixed $W$ there is a hardening for increasing $Q^2$ .

For all bins with medium $Q^2$ and small $x$ (excluding bins 6 and 9) the CJC acceptance reaches further into the central rapidity region. Here the $p_T$ spectrum can also be measured for $0.5 < \eta < 1.5$ (see Figure 3), where the difference between the two types of models becomes stronger. The failure of the event generators which are based upon leading log DGLAP parton showers to describe the hard component present in the data now becomes even more prominent. ARIADNE with more gluon radiation describes the data well. Comparing the $p_T$ spectra for the two pseudorapidity intervals in the same kinematic bin (bin 3, low $x$ ), it is found that the spectrum becomes harder when one moves towards the current direction, see Fig. 4 d. This is not surprising, as the average $k_T$ of the gluons emitted in both scenarios, DGLAP and BFKL, increases along the ladder towards the photon vertex [3]. Also radiation associated with the current system with the virtuality of the photon $Q^2$ as a scale is expected to contribute more in that direction.

It has been studied whether LEPTO parameters can be modified to obtain a better description of the data. Some improvement over the standard settings was obtained by using a fragmentation parameter set tuned to LEP data [33] ("ALEPH set"). The most sensitive parameter however is the virtuality cut-off below which final state radiation is not allowed, and fragmentation takes over. When this parameter is changed from its default value of 1 GeV$^2$ to 3 GeV$^2$ , the $p_T$ spectra for $1.5 < \eta < 2.5$ are much better described. However, this setting has to be rejected as unphysical, because the observed scaling violations in the Feynman -$x_F$ spectra [8, 34] can no longer be reproduced. In addition, the $p_T$ spectra measured more centrally at $0.5 < \eta < 1.5$ are still much harder than in the modified model. We conclude that the rapidity bin $1.5 < \eta < 2.5$ is not central enough to be unaffected by the current system dynamics. For the more central bin $0.5 < \eta < 1.5$ this dependence is much reduced.

In order to obtain a measure for the hardness of the $p_T$ spectrum over the entire range of pseudorapidity accessible by this analysis, the average multiplicity of charged particles with $p_T > 1$ GeV is measured (see Fig. 5) as a function of pseudorapidity. The surplus of hard particles in the data over the DGLAP-like models at small $x$ and away from the current region is obvious. The best description of the data is achieved by ARIADNE. In contrast to the multiplicity of hard particles, the overall multiplicity, which is dominated by soft particles, is much better (though not perfectly) described by all models, see Fig. 6. Only Herwig overshoots the data considerably at small $x$ and towards the remnant.

The discrimination between the different scenarios can be enhanced by selecting events with large hadronic activity, because in those events also the partonic activity is large for the model with unsuppressed radiation, as opposed to the other models [13]. Here the transverse energy measured with the calorimeter in the $\eta$ range from 0.0 to 2.0 is required to be larger than 6 GeV. The $p_T$ distribution of the track with the largest transverse momentum $p_T^{\max}$ in the range $0.5 < \eta < 1.5$ in each event is then determined, see Fig. 7. In that way one can reveal the correlation between large $E_T$ production, which could be produced by many soft particles in the hadronization, and high $p_T$ particles, which indicate hard parton radiation. The events contain much harder particles than are produced in the models MEPS and HERWIG. Again, ARIADNE with enhanced parton radiation describes the data very well. The discrepancy between the data and ARIADNE on one side, and LEPTO and HERWIG on the other side, becomes larger for smaller $x$ and $Q^2$ .

So far we concentrated on the deviations observed at low $x$, because there the parton cascade between the current and the remnant is most developed, and the difference between the BFKL- and DGLAP-type behaviours is expected to be strongest. It is noteworthy that the colour dipole model (ARIADNE) is able to describe both kinematic regions at large and small $x$ simultaneously.

# 5 Conclusions

Transverse momentum spectra of charged particles in deep inelastic scattering have been measured as a function of $x$ and $Q^2$ in between the current and the remnant fragmentation region. In addition, the average charged particle multiplicity has been measured as a function of pseudorapidity. The data are used to probe the underlying parton dynamics in deep inelastic scattering at small $x$ . The data are compared to QCD models incorporating different schemes for parton evolution in the proton, namely $k_T$ ordered resp. unordered parton emissions, leading to either suppressed or abundant parton radiation between the current system and the remnant. In that respect they can be considered as representatives of the leading log DGLAP resp. BFKL evolutions. At large $x$ , all models provide an overall satisfactory description of the measured $p_T$ spectra. At small $x$ however and at central rapidity the $p_T$ distributions are significantly harder than expected from the models with suppressed radiation. The unsuppressed scenario, as realized in a colour dipole radiation model, is able to describe the data. We conclude that for the description of the hadronic final state in deep inelastic scattering contributions other than the conventional leading log DGLAP ones as implemented in the current QCD models are neccessary. The observed hard $p_T$ spectra indicate hard parton radiation, which could be provided by BFKL-type contributions. Further interpretation of the data has to await firm QCD calculations and a Monte Carlo model which explicitly includes the BFKL terms. The DGLAP equations can be shown to hold rigorously - within its region of validity - for the totally inclusive structure function evolution. It would now be worthwhile to reexamine the question to what extent the probabilistic use of the DGLAP splitting functions in a parton shower approach is justified to calculate hadronic final state observables.

**Acknowledgements.** We are grateful to the HERA machine group whose outstanding efforts made this experiment possible. We appreciate the immense effort of the engineers and technicians who constructed and maintained the detector. We thank the funding agencies for financial support. We acknowledge the support of the DESY technical staff. We also wish to thank the DESY directorate for the hospitality extended to the non-DESY members of the collaboration.

# References


[1] Yu. L. Dokshitzer, Sov. Phys. JETP 46 (1977) 641;
V.N. Gribov and L.N. Lipatov, Sov. J. Nucl. Phys. 15 (1972) 438 and 675;
G. Altarelli and G. Parisi, Nucl. Phys. 126 (1977) 297 .

[2] E.A. Kuraev, L.N. Lipatov and V.S. Fadin, Sov. Phys. JETP 45 (1972) 199;
Y.Y. Balitsky and L.N. Lipatov, Sov. J. Nucl. Phys. 28 (1978) 282 .

[3] J. Bartels, H. Lotter, Phys. Lett. B309 (1993) 400;
A. Mueller, Columbia preprint CU-TP-658 (1994);
J. Bartels, H. Lotter and M. Vogt, DESY-95-224 .

[4] H1 Collab., T. Ahmed et al., Nucl. Phys. B439 (1995) 471 .

[5] ZEUS Collab., M. Derrick et al., Z. Phys. C65 (1995) 379; Z. Phys. C69 (1996) 607 .

[6] A.J. Askew, J. Kwieciński, A.D. Martin, P.J. Sutton, Phys. Lett. B325 (1994) 21 .

[7] M. Glück, E. Reya, A. Vogt, Z. Phys. C67 (1995) 433 .

[8] H1 Collab., I. Abt et al., Z. Phys. C63 (1994) 377 .

[9] J. Kwieciński, A.D. Martin, P.J. Sutton and K.Golec-Biernat, Phys. Rev. D50 (1994) 217;
K.Golec-Biernat, J. Kwieciński, A.D. Martin and P.J. Sutton, Phys. Lett. B335 (1994) 220 .

[10] H1 Collab., S. Aid et al., Phys. Lett. B356 (1995) 118 .

[11] M. Kuhlen, MPI-PhE/95-19 (1995), hep-ex/9508014; Proc. of the Workshop on Deep Inelastic Scattering and QCD - DIS95, Paris, April 1995, eds. JF. Laporte and Y. Sirois, p. 345 .

[12] A. Edin, G. Ingelman and J. Rathsman, Phys.Lett. B366 (1996) 371;
A. Edin, G. Ingelman and J. Rathsman, DESY 96-060 .

[13] M. Kuhlen, MPI-PhE/96-10 (1996), hep-ph/9606246 .

[14] G. Ingelman, Proc. of the Workshop on Physics at HERA, Hamburg 1991, eds. W. Buchmüller and G. Ingelman, vol. 3, p. 1366 .

[15] G. Gustafson, Ulf Petterson, Nucl. Phys. B306 (1988);
G. Gustafson, Phys. Lett. B175 (1986) 453;
B. Andersson, G. Gustafson, L. Lönnblad, Ulf Petterson, Z. Phys. C43 (1989) 625 .

[16] L. Lönnblad, Computer Phys. Comm. 71 (1992) 15 .

[17] T. Sjöstrand, Comp. Phys. Comm. 39 (1986) 347;
T. Sjöstrand and M. Bengtsson, Comp. Phys. Comm. 43 (1987) 367;
T. Sjöstrand, CERN-TH-6488-92 (1992) .

[18] G. Marchesini, B.R. Webber, G. Abbiendi, I.G. Knowles, M.H. Seymour and L. Stanco, Computer Phys. Comm. 67 (1992) 465 .

[19] M. Seymour, Lund preprint LU-TP-94-12 (1994);
M. Seymour, Nucl. Phys. B436 (1995) 443 .

[20] B.R. Webber, Nucl. Phys. B238 (1984) 492 .

[21] L. Lönnblad, Z. Phys. C65 (1995) 285;
A. H. Mueller, Nucl. Phys. B415 (1994) 373;
L. Lönnblad, CERN-TH/95-95 .

[22] T. Carli, Proc. of the DIS96 Workshop, Rome 1996 .

[23] ZEUS Collab., M. Derrick et al., Phys. Lett. B315 (1993) 481;
H1 Collab., T. Ahmed et al., Nucl.Phys. B429 (1994) 477 .

[24] A.D. Martin, W.J. Stirling and R.G. Roberts, Proc. of the Workshop on Quantum Field Theory and Theoretical Aspects of High Energy Physics, eds. B. Geyer and E.M. Ilgenfritz (1993) p. 11 .

[25] H1 Collab., I. Abt et al., DESY 93-103 (1993) .

[26] H1 Calorimeter Group, B. Andrieu et al., Nucl. Instr. and Meth. A336 (1993) 460 .

[27] H1 Calorimeter Group, B. Andrieu et al., Nucl. Instr. and Meth. A336 (1993) 499 .

[28] H1 BEMC Group, J. Bán et al., Nucl. Instr. and Meth. A 372 (1996) 399 .

[29] K. Charchula, G. Schuler, H. Spiesberger, CERN-TH.7133/94 .

[30] A. Kwiatkowski, H. Spiesberger and H.-J. Möhring, Computer Phys. Comm. 69 (1992) 155 .

[31] H1 Collaboration, S. Aid et al., DESY 96-039 .

[32] H1 Collab., S. Aid et al., Phys. Lett. B358 (1995) 412 .

[33] I.G. Knowles et al., hep-ph9601212 .

[34] ZEUS Collab., M. Derrick et al., Z. Phys. C70 (1996) 1 .

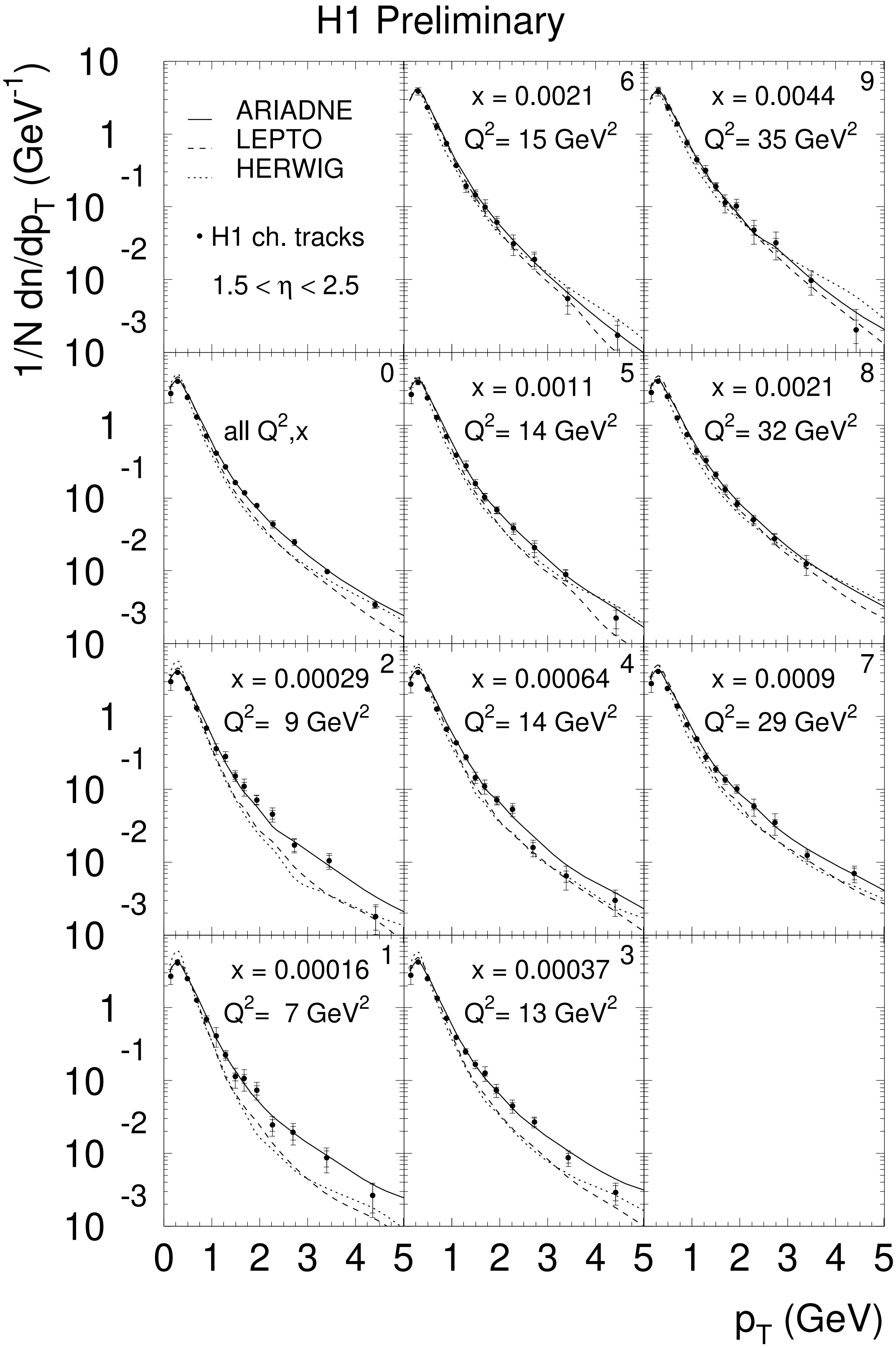


Figure 2: The CMS charged particle transverse momentum spectra in the pseudorapidity interval $\eta$ from 1.5 to 2.5. Shown are data for nine different kinematic bins (see Table 1) plus the combined sample (bin 0). For comparison, the models ARIADNE (full line), LEPTO (dashed) and HERWIG (dotted) are overlayed. The mean values of $x$ and $Q^2$ are indicated.

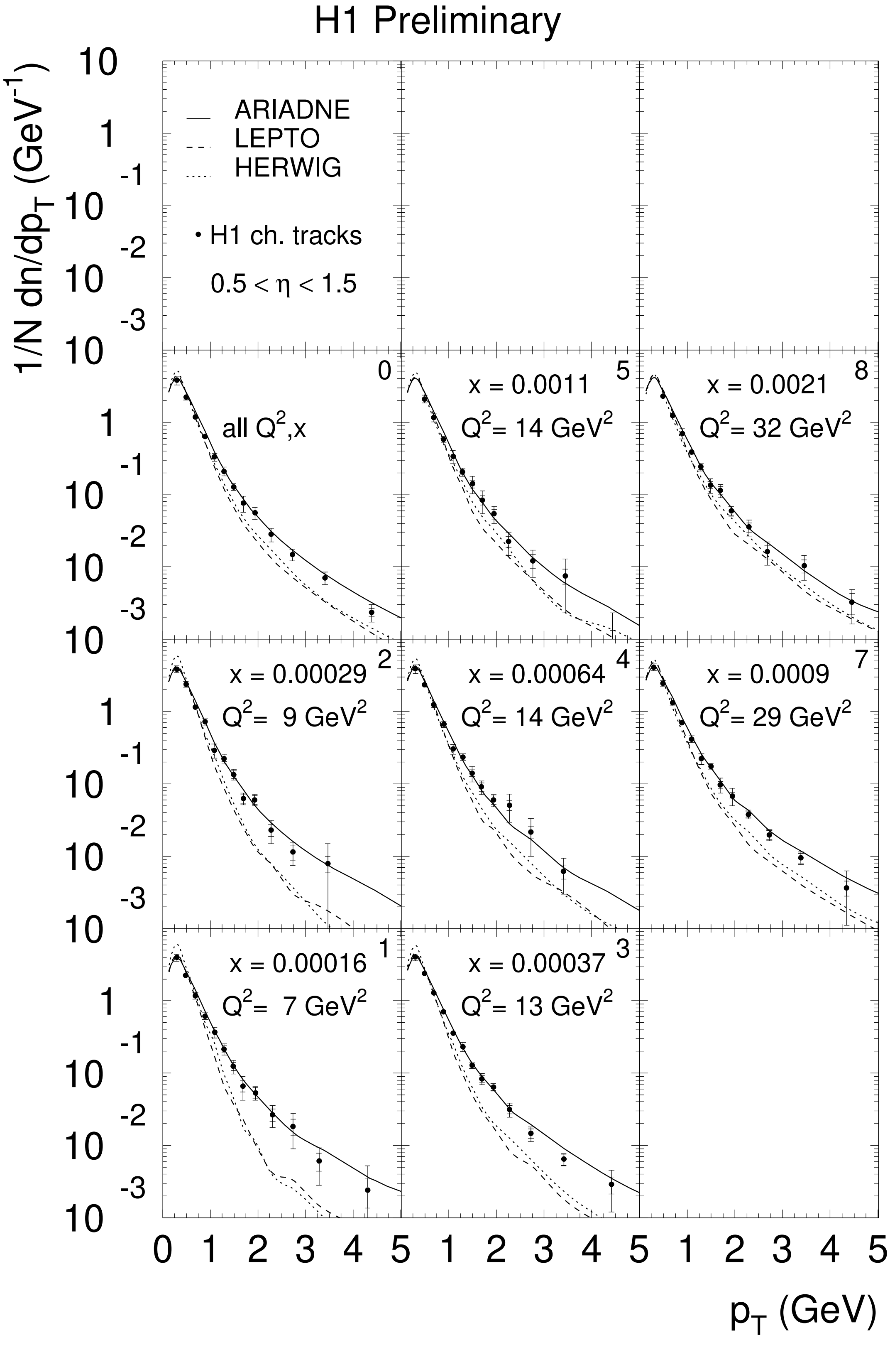


Figure 3: The CMS charged particle transverse momentum spectra in the pseudorapidity interval $\eta$ from 0.5 to 1.5. Shown are data for seven different kinematic bins (see Table 1) plus the combined sample (bin 0). For comparison, the models ARIADNE (full line), LEPTO (dashed) and HERWIG (dotted) are overlayed. The mean values of $x$ and $Q^2$ are indicated.

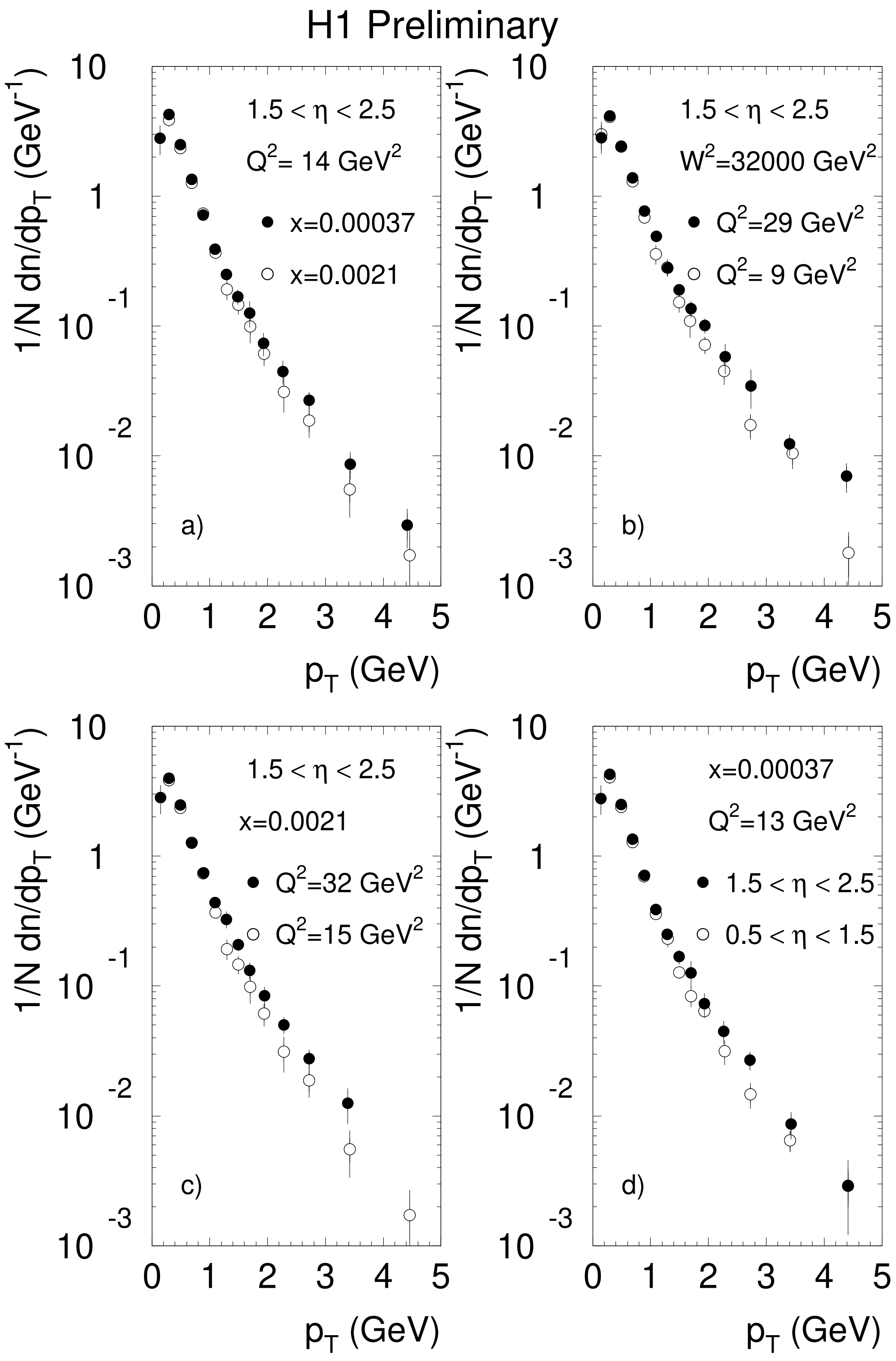


Figure 4: **a)** Comparison of the $p_T$ spectra at high $x$ (bin 6) and at low $x$ (bin 3) for fixed (intermediate) $Q^2$ . **b)** Comparison of the $p_T$ spectra at two different $Q^2$ values (bins 2 and 7) for fixed (large) $W$. **c)** Comparison of the $p_T$ spectra at two different $Q^2$ values (bins 6 and 8) for fixed (large) $x$. **d)** Comparison of the $p_T$ spectra at in two different $\eta$ intervals in the kinematic bin 3 (low $x$ , intermediate $Q^2$ ). The mean values of $x$ and $Q^2$ are indicated in the figures.

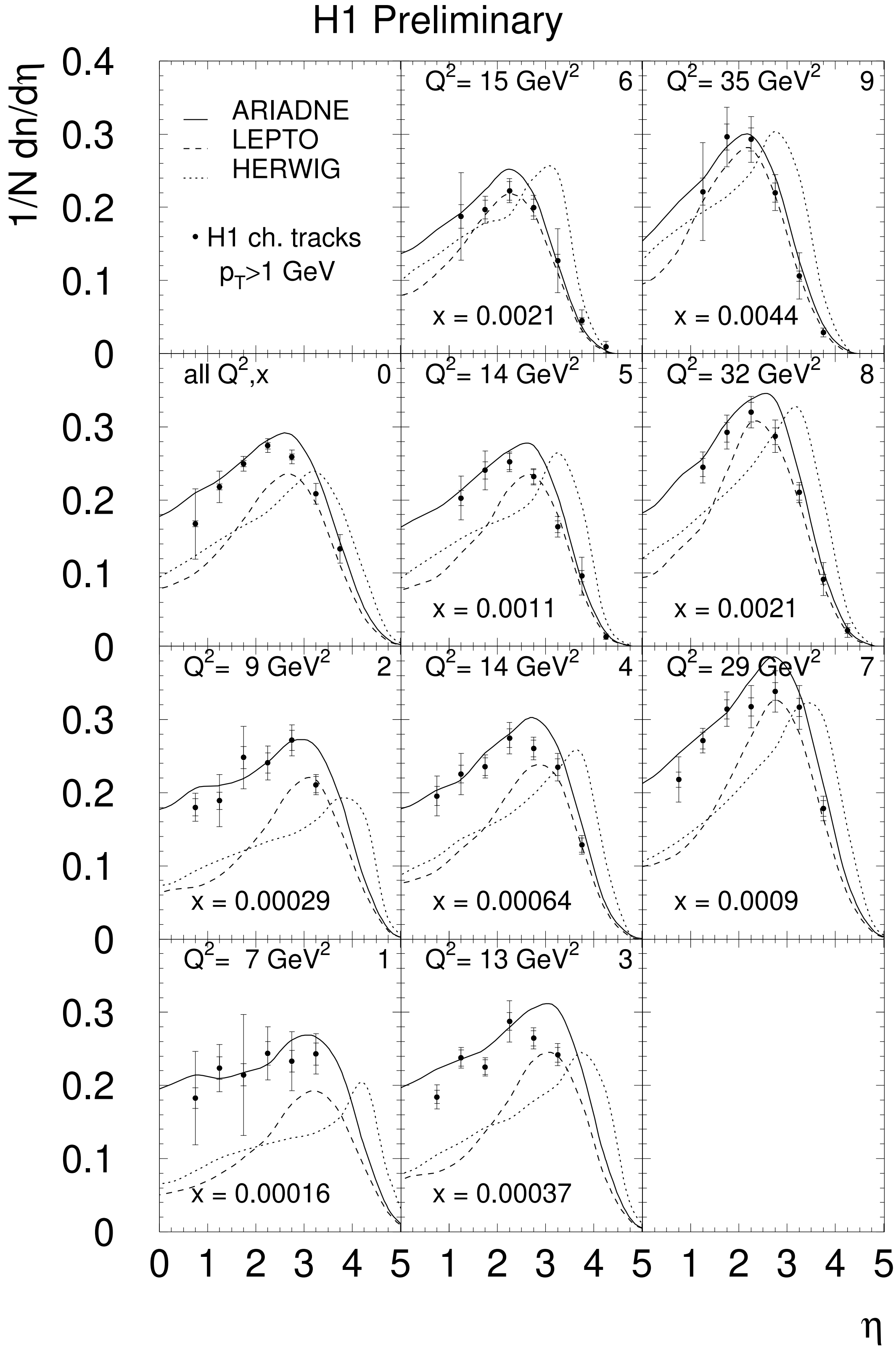


Figure 5: The CMS pseudorapidity spectra for charged particles with $p_T > 1 GeV$. The proton remnant direction is to the left. Shown are data for nine different kinematic bins (see Table 1) plus the combined kinematic region (bin 0). For comparison, the models ARIADNE (full line), LEPTO (dashed) and HERWIG (dotted) are overlayed. The mean values of $x$ and $Q^2$ are indicated.

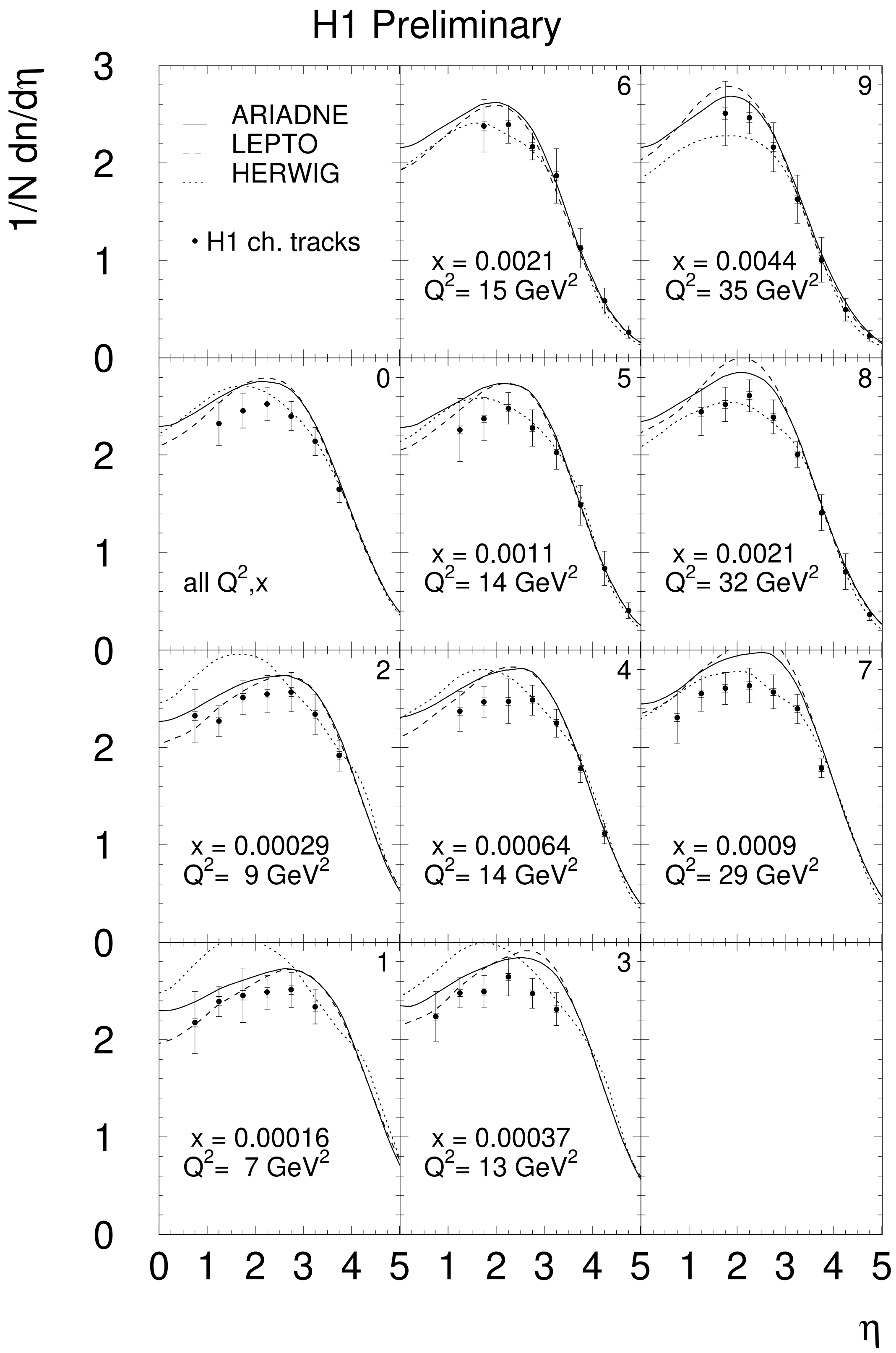


Figure 6: The CMS pseudorapidity spectra for all charged particles. The proton remnant direction is to the left. Shown are data for nine different kinematic bins (see Table 1) plus the combined kinematic region (bin 0). For comparison, the models ARIADNE (full line), LEPTO (dashed) and HERWIG (dotted) are overlayed. The mean values of $x$ and $Q^2$ are indicated.

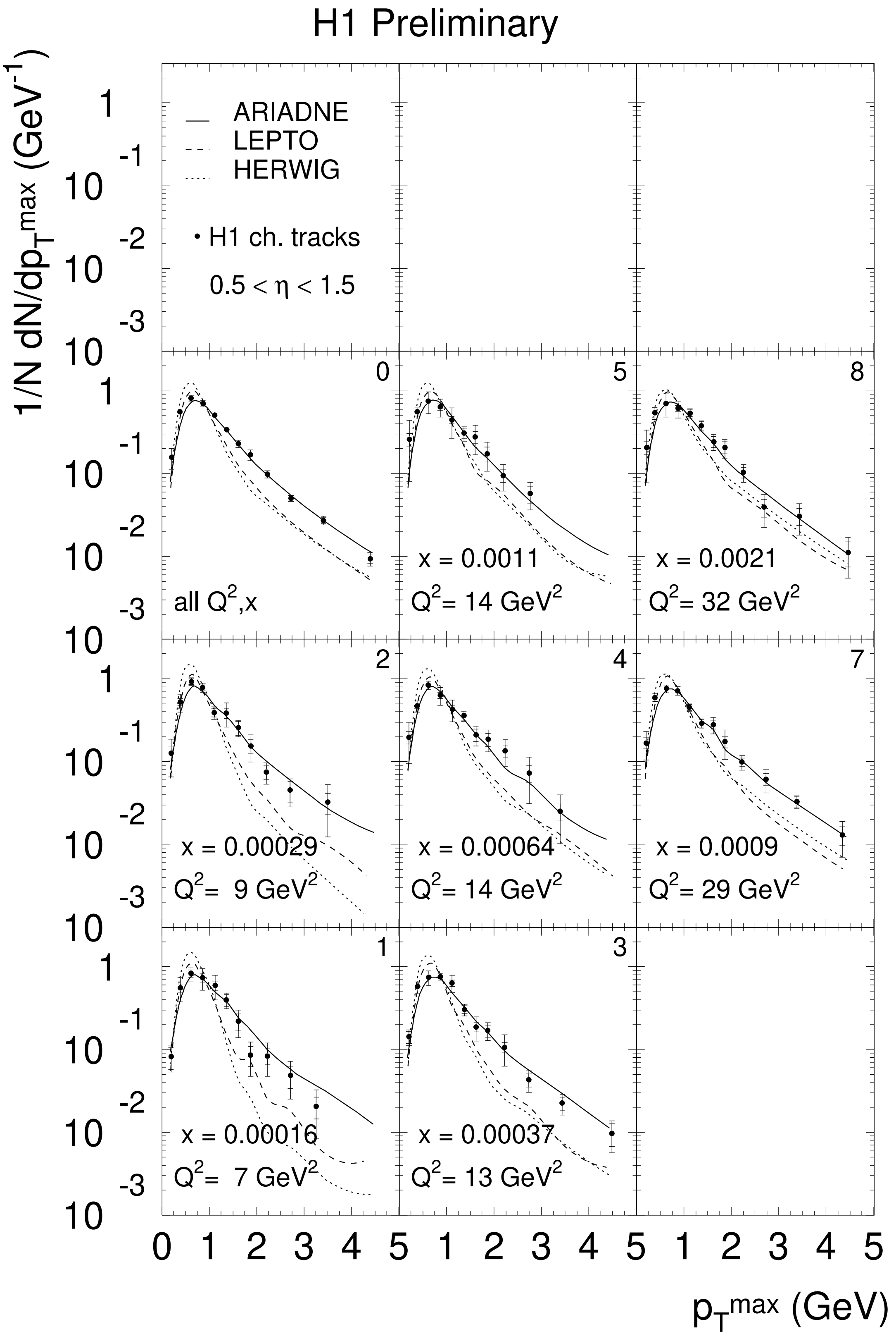


Figure 7: The $p_T^{\max}$ distribution as explained in the text, for the interval $0.5 < \eta < 1.5$. Shown are data for seven different kinematic bins (see Table 1) plus the combined kinematic region (bin 0). For comparison, the models ARIADNE (full line), LEPTO (dashed) and HERWIG (dotted) are overlayed. The mean values of $x$ and $Q^2$ are indicated.